Published in final edited form as:
Biochemistry. 2006 October 31; 45(43): 13083–13092. doi:10.1021/bi060948r.

The Affinity of Copper Binding to the Prion Protein Octarepeat Domain: Evidence for Negative Cooperativity†

Eric D. Walter, **Madhuri Chattopadhyay**, and **Glenn L. Millhauser***
Department of Chemistry and Biochemistry, University of California, Santa Cruz, California 95064

Abstract

The prion protein (PrP) binds Cu^{2+} in its N-terminal octarepeat domain, composed of four or more tandem PHGGGWGQ segments. Previous work from our laboratory demonstrates that copper interacts with the octarepeat domain through three distinct coordination modes at pH 7.4, depending upon the precise ratio of Cu^{2+} to protein. Here, we apply both electron paramagnetic resonance (EPR) and fluorescence quenching to determine the copper affinity for each of these modes. At low copper occupancy, which favors multiple His coordination, the octarepeat domain binds Cu^{2+} with a dissociation constant of 0.10 (±0.08) nM. In contrast, high copper occupancy, involving coordination through deprotonated amide nitrogens, exhibits a weaker affinity characterized by dissociation constants in the range of 7.0–12.0 μM. Decomposition of the EPR spectra reveals the proportions of all coordination species throughout the copper concentration range and identifies significant populations of intermediates, consistent with negative cooperativity. At most copper concentrations, the Hill coefficient is less than 1.0 and approximately 0.7 at half copper occupancy. These findings demonstrate that the octarepeat domain is responsive to a remarkably wide copper concentration range covering approximately 5 orders of magnitude. Consideration of these findings, along with the demonstrated ability of the protein to quench copper redox activity at high occupancy, suggests that PrP may function to protect cells by scavenging excess copper.

The prion protein (PrP)[1] is responsible for a novel class of infectious, neurodegenerative diseases collectively known as the transmissible spongiform encephalopathies (TSEs) (1–3). The TSEs include scrapie in sheep, mad cow disease (bovine spongiform encephalopathy, BSE), chronic wasting disease (CWD) in deer and elk, and Creutzfeldt–Jakob disease (CJD) in humans. The normal cellular form of the prion protein, referred to as PrP^C, is found in a wide range of tissues of all mammalian and avian species. A misfolding event converts the protein to the infectious, β-sheet-rich scrapie form (PrP^{Sc}) responsible for the TSEs.

PrP^C is a GPI-anchored glycoprotein expressed in abundance on the surface of neurons, predominantly on presynaptic membranes (4,5). The mature form of PrP, consisting of residues 23–231 in hamster, has a globular C-terminal domain and a largely unstructured N-terminal domain (6) (Figure 1). The C-terminal domain (residues 125–231) contains three α helices, two of which are stabilized by a single interhelical disulfide bond, and a small antiparallel β sheet. The flexible N-terminal domain is glycine-rich and highly flexible. Within the flexible N-terminal region of PrP is the octarepeat domain, composed of four or five highly conserved, contiguous repeats of the eight-residue sequence PHGGGWGQ. The physiological function

†This work was supported by NIH Grant GM 65790 and NSF Instrumentation Grant DBI-0217922 (to G.L.M.).

* To whom correspondence should be addressed. Telephone: (831) 459-2176. Fax: (831) 459-2935. glennm@chemistry.ucsc.edu.

[1]Abbreviations: PrP, prion protein; PrP^C, cellular isoform of PrP; PrP^{Sc}, scrapie isoform of PrP; TSE, transmissible spongiform encephalopathy; CJD, Creutzfeldt–Jakob disease; PrP(57–91), residues 57– 91 of PrP; EPR, electron paramagnetic resonance; K_d, dissociation constant; *n*, Hill coefficient; SOD, superoxide dismutase; Sar, sarcosine (*N*-methyl glycine); NEM, *N*-ethylmorpholine; DTAB, dodecyltrimethylammonium bromide.

of PrP^C is unknown, but recent investigations focus on the ability of the octarepeat domain to take up copper (5,7–11). PrP^C protects against apoptosis (12) and radical-mediated oxidative damage (13,14) and even stimulates nerve cell growth and development (15). Several copper-specific neuroprotective mechanisms have been proposed, including enzymatic function as a superoxide dismutase (SOD) (16), copper sequestration to inhibit deleterious oxidative chemistry (9,17), and copper-dependent cellular signaling (5,13).

To establish a molecular basis for the neuroprotective role of PrP, recent studies have focused on the elucidation of the chemical environment of the Cu^{2+}-binding sites. Research from our laboratory demonstrates that, at pH 7.4, each HGGGW segment within the octarepeat domain binds one Cu^{2+} at saturation (18–20). In more recent work, we have shown that the octarepeat domain takes up Cu^{2+} in three distinct coordination modes, referred to as components 1, 2, and 3, controlled by the precise molar ratio of Cu^{2+} to protein, as shown in Figure 1 (17). These coordination modes are clearly discernible by a combination of electron paramagnetic resonance (EPR) techniques, including multifrequency and pulsed EPR. The component 3 coordination mode, which is observed at low copper occupancy, involves three to four octarepeats binding a single Cu^{2+} through the histidine imidazoles. At intermediate copper occupancy, the coordination mode switches to a mixture of components 2 and 1. In component 2, Cu^{2+} is bound to both the imidazole nitrogen and deprotonated amide nitrogen of histidine within a single octarepeat. A second imidazole nitrogen from a neighboring octarepeat is postulated to bind Cu^{2+} in the axial position (17). Component 1 arises at full copper occupancy and involves Cu^{2+} coordination to the HGGGW residues within each octarepeat through an imidazole nitrogen of histidine, deprotonated amide nitrogens from the two following glycines, and the amide carbonyl oxygen from the second glycine. The Trp participates through the formation of a hydrogen bond from the indole NH to an axially coordinated water (19).

Determining the precise affinity for copper binding to PrP is essential for assessing the normal function of the protein. For an enzyme, one would expect high affinity, reflected through a low dissociation constant (K_d) (21), whereas buffering or sensing would require a lower affinity, with a K_d near the concentration of extracellular copper (22). Unfortunately, investigations into the dissociation constant and the mechanism of copper uptake reveal highly disparate outcomes depending upon the measurement technique and the particular PrP construct (8,10, 21–25). Current estimates place K_d between 10^{-6} M (10,22,23) and 10^{-14} M (21,24), an experimental uncertainty of 8 orders of magnitude. For example, mass spectrometry studies on PrP(57–91), encompassing all of the octarepeats, finds a dissociation constant of 0.2 μM for the first bound Cu^{2+}, with the K_d increasing to 12 μM for the fourth Cu^{2+} (10). Similar micromolar affinities have been identified using amino acid competition studies, as detected by circular dichroism (CD) (23). Alternatively, binding curves determined from tryptophan fluorescence quenching from Cu^{2+} report a very high-affinity site with a K_d of 8×10^{-15} M (8 fM) in PrP(57–98) (24). Isothermal titration calorimetry (ITC) and competitive metal capture analysis (CMCA) also support the presence of a high-affinity Cu^{2+}-binding site in the octarepeat region (21).

Several reports suggest that the octarepeat domain takes up Cu^{2+} with positive cooperativity (8,22,25). For instance, equilibrium dialysis measurements performed on PrP(23–98) find a half-maximal binding at 5.9 μM and a Hill coefficient (n) of 3.4, indicating a very strong positive cooperativity through the micromolar range (8). Similar results were obtained from CD measurements of the d–d absorption band at 570 nm, arising from Cu^{2+} binding to PrP (58–91) (25). The CD signal increases in a sigmoidal fashion, consistent with positive cooperativity. In support of these studies, fluorescence quenching measurements suggest that binding occurs with a half-maximal value of 5.5 μM and a Hill coefficient of 2.4 (22). On the other hand, electrospray ionization (ESI) mass spectrometry performed on PrP(57–91) found

a progressive decrease in the binding affinity as a function of the copper load, perhaps suggesting negative cooperativity (10).

Positive cooperativity would exert a profound affect on the distribution of copper-occupied states. Specifically, concentrations of unbound and fully copper-occupied PrP should be dominant and substantially greater than partially copper-occupied proteins (26). This is certainly the case for oxygen binding to hemoglobin, which is characterized by a Hill coefficient of 2.8. This suppression of intermediate states is in contrast to the behavior recently observed by our laboratory in the elucidation of the three copper-dependent binding components in the octarepeat domain (17). EPR spectra suggest large populations of partially occupied intermediates, quite the opposite of positive cooperativity.

The identification of distinct octarepeat binding modes in PrP motivates a re-evaluation of the affinity of the protein for copper. The individual modes may have widely differing dissociation constants and, if so, would help explain the wide discrepancy among previously published values. In addition, determining the affinity for each binding mode provides a quantitative assessment of cooperative copper uptake. Here, we use fluorescence quenching and EPR measurements on the octarepeat domain, along with a library of octarepeat-derived constructs and selective chelators in competition studies, to determine the affinity for the copper-binding components 1, 2, and 3. Next, we develop and apply an EPR approach for following the populations of the components as a function of copper occupancy to evaluate cooperative uptake. Using the population distribution, we then determine the Hill coefficient as a function of copper occupancy. In contrast to previous published measurements, we find that the affinity ranges from approximately 0.1 nM at low Cu^{2+} occupancy to 10 μM at high Cu^{2+} occupancy, with a Hill coefficient of less than 1.0 indicative of negative cooperativity. For select cases, we reconcile these findings with those that were previously interpreted as providing evidence of positive cooperativity.

Materials and Methods

Peptide Synthesis and Purification

All peptides were prepared with N-terminal acetylation and C-terminal amidation, using fluorenylmethoxycarbonyl (Fmoc) methods, as described previously (17–20). N-Methylated amino acids were incorporated using a custom coupling procedure (17). Peptides were purified by reverse-phase high-performance liquid chromatography (HPLC) and characterized by mass spectrometry.

EPR

All samples were prepared with degassed buffer containing 25 mM *N*-ethylmorpholine (NEM) buffer and 20% glycerol (v/v), where the glycerol served as a cryoprotectant (18). X-band spectra (frequency of 9.43 GHz, microwave power in the range of 0.6–5.0 mW, and modulation amplitude of 5.0 G) were acquired at approximately 125 K using a Bruker EleXsys 500 spectrometer and an SHQ (Bruker) cavity equipped with a variable temperature controller. Composite spectra were fit to eq 4 using non-negative least-squares (NNLS) routines in the Matlab program suite.

CD

CD spectra in the visible region were acquired using a 1.0 cm path-length square cell and presented as a sum of four scans. Samples were prepared in a buffer containing 25 mM NEM at pH 7.4 and 20% glycerol (v/v) using 300 μM peptide. Cu^{2+} was added from a stock prepared in the same buffer. The concentration of bound Cu^{2+} was determined from double integration of EPR spectra for the corresponding sample.

Fluorescence

Fluorescence spectroscopy was carried out using a Jobin Yibon Fluoromax-3 instrument. All titrations were performed in syringe-filtered (0.22 μm) and degassed NEM buffer containing 25 mM NEM, 1 mM dodecyltrimethylammonium bromide (DTAB), and 100 mM NaCl at pH 7.4. Cu^{2+} was added from a $CuSO_4/CuCl_2$ stock prepared in Nanopure water and thoroughly mixed by successive inversions of the tube followed by pipeting in and out with a glass Pasteur pipet. Care was taken to avoid frothing and precipitation. The excitation wavelength was set to 265 nm, and emission spectra were averaged over three scans acquired from 280 to 450 nm. Excitation and emission slit widths were set to 5 nm. A blank spectrum of the corresponding amount of Cu^{2+} added to NEM buffer and scanned under identical conditions was subtracted from each experimental spectrum. Data were processed using KaleidaGraph (Synergy Software).

Results

The octarepeat domain, within the flexible N-terminal region of PrP, represents a unique Cu^{2+}-binding segment. In hamster and human PrP, this region encompasses residues 60–91 and consists of four tandem repeats of the sequence PHGGGWGQ. Previous work from our lab shows that the specific binding mode is highly dependent upon the number of bound copper equivalents per protein (17). Molecular features for these different binding modes are shown in Figure 1. Here, we extend our previous structural work to determine the copper affinities for each individual binding mode. In addition, EPR spectroscopic signatures allow us to determine the populations of each binding mode as a function of copper occupancy. When this fundamental information is taken together, it yields the affinity as a function of copper occupancy and, consequently, the cooperativity of copper uptake.

Dissociation Constants of Components 1, 2, and 3

Each octarepeat segment contains a single tryptophan residue. Bound Cu^{2+} quenches tryptophan fluorescence and thus provides a convenient and proven method for monitoring copper uptake (22,24,27). Although affinity, as reflected through dissociation constants, is ideally determined from the full-length protein, several aspects of PrP complicate this approach. First, as determined by our lab and others, there are one or more copper-binding sites outside of the octarepeat domain (20,28). Next, copper binding within the octarepeat domain is heterogeneous, passing through a series of intermediates before reaching saturation at 1 equiv per octapeptide segment (17). The best approach, therefore, is to determine the dissociation constant for a series of constructs, where each takes up copper in a single binding mode, and then test the resulting affinities in the intact octarepeat domain, PrP(23–28, 57–91). To achieve this objective, we use the full octarepeat domain, as well as octarepeat domain constructs developed in our previous studies (17) (Table 1). Briefly, PrP(23–28, 57–91) encompasses the entire octarepeat domain and, when challenged with up to a single Cu^{2+} equivalent, binds strictly as component 3. The short N-terminal segment of this peptide, residues 23–28, is included to improve solubility. The peptide HGXGWGQPHGXGW, where X = sarcosine (Sar), is limited to the component 2 mode because it provides two His residues but lacks two critical backbone amides required for component 1. Finally, the fundamental pentapeptide HGGGW binds Cu^{2+} strictly as component 1.

Cu^{2+} quenches tryptophan fluorescence through both direct binding and collisions with aqueous, unbound copper. The former process gives rise to a saturable binding curve, given by eq 1

$$\frac{F_0 - F}{F_0} = \frac{\left[Cu^{2+}\right]_{free}}{K_d + \left[Cu^{2+}\right]_{free}} \quad (1)$$

where F_0 and F are the unquenched ($[Cu^{2+}] = 0.0$) and quenched fluorescence intensities, respectively. Collisional quenching is linear with respect to F_0/F and dominates at concentrations where $[Cu^{2+}] \gg K_d$ (22). Effects from collisional quenching were removed from the experimental data by subtracting the slope of a linear fit to F_0/F for $[Cu^{2+}] > 200$ μM. (We did not observe nonlinear behavior in plots of F_0/F at high $[Cu^{2+}]$ that might arise from a combination of static and collisional quenching.) The corrected data, along with fits to eq 1, are shown in parts A and B of Figure 2. For all measurements of component 1 and 2 coordination, peptide concentrations were kept well below the anticipated dissociation constants, thus allowing the use of the approximation $[Cu^{2+}]_{free} \gg [Cu^{2+}]_{total}$. To test the robustness of this approach, K_d values were determined at several peptide concentrations, as reported in Table 2. There are only minor random variations in K_d, and these variations are independent of the peptide concentration. The dissociation constant for Cu^{2+} binding in component 1 (using the peptide HGGGW) is 7.2 μM, and replicate experiments on HGXGWGQPHGXGW, which binds in the component 2 mode, give a K_d of 12.6 μM.

Unfortunately, binding detected through fluorescence quenching is not suitable for determining the K_d of component 3. The octarepeat construct PrP(23–28, 57–91) binds in the component 3 mode up to 1.0 equiv of copper but, when challenged with greater than 1 equiv, proceeds to the other binding modes. No octarepeat construct gives component 3 exclusively, through a wide copper concentration range. As a preliminary test of relative affinity, PrP(23–28, 57–91) with a single Cu^{2+} equivalent was challenged with a 500-fold excess of HGGGW and monitored by EPR. Interestingly, Cu^{2+} remained quantitatively bound to PrP-(23–28, 57–91) in the component 3 mode, suggesting that the K_d of component 3 is subnanomolar. Meaningful fluorescence quenching experiments using the formalism above are only achievable when the peptide concentration is less than K_d. As such, the tentative subnanomolar K_d of component 3 is below the fluorescence detection limit for the endogenous tryptophans.

To quantitatively assess component 3 binding, we developed a new technique that uses EPR in conjunction with copper chelators of known affinity. The PrP peptide, specific chelator, and a limiting amount of copper are mixed and allowed to come to equilibrium. The concentration of each Cu^{2+}-bound species is determined from their contribution to the composite EPR spectrum. For the simplest case of a competitive chelator that binds copper in a 1:1 ratio, the K_d of the peptide is calculated using

$$K_d = \frac{[P][Cu]}{[PCu]}; \quad K_{dc} = \frac{[C][Cu]}{[CCu]}; \quad K_d = K_{dc}\frac{[P][CCu]}{[C][PCu]} \quad (2)$$

where P is the peptide, C is the chelator, and K_{dc} is the known dissociation constant for the copper–chelate complex. For a bischelator that binds in a 2:1 mode (with the chelator concentration $\gg K_{dc2}$), the K_d of the peptide can be related to β

$$K_{dc1} = \frac{[C][Cu]}{[CCu]}; \quad K_{dc2} = \frac{[C][CCu]}{[C_2Cu]}; \quad \beta = K_{dc1}K_{dc2}; \quad K_d = \beta\frac{[P][C_2Cu]}{[C]^2[PCu]} \quad (3)$$

While the concentrations of the copper-bound PrP construct and chelator are measured directly, the concentrations of the copper-free species must be calculated as the difference between the total and bound species. Even though the above equations are correct regardless of the concentration, spurious results may occur if the concentration of any species is too low and thus not accurately determined. To avoid this situation, copper is held to be the limiting reagent so that the free peptide and competing chelator are at concentrations in the same range as the respective copper-bound species. Also, the copper affinities of the peptide and chelator cannot be so different that essentially only one copper species is formed (at measurable concentrations).

For these experiments, amino acids serve as excellent chelators. We identified a set of four amino acids (Arg, Asn, Gly, and Met) with widely varying copper dissociation constants (Table 3). Under the conditions of our experiments, all of these species bind 2:1 with Cu^{2+} (see eq 3) and give EPR spectra that reflect only two copper-bound species: chelator and PrP(23–28, 57–91) (Figure 3A). In contrast, many other copper chelators had to be disqualified because of the formation of ternary complexes with copper simultaneously bound to both the PrP peptide and chelator. These include ethylenediaminetetraacetic acid (EDTA), 1,10-phenanthroline, nitrilotriacetic acid, neocuproine, bathocuproine, triphosphate, and others. For these chelators, the presence of ternary compounds was directly verified by ESI mass spectrometry.

EPR spectra from competition experiments were fit to a superposition of two spectra and integrated to determine the respective bound copper concentrations, as shown for one example in Figure 3A. Results obtained for several different copper chelators, over a range of concentrations, are shown in Figure 3B. Each data point represents a single K_d determination. Except for asparagine, the data do not exhibit any systematic concentration dependence, which attests to the robustness of the technique. Measured K_d values are clustered around 10^{-10} M (0.10 nM), with low asparagine concentrations giving slightly higher K_d values and methionine giving slightly lower values. Figure 3C shows average K_d values determined for each of the amino acid chelators. The mean values for K_d fall in the range of 0.02–0.20 nM, although determinations using asparagine as the competitor give greater scatter. The average dissociation constant for component 3 is 0.10 ± 0.08 nM. This shows that component 3 binds copper with an affinity that is nearly 5 orders of magnitude greater than that for component 1.

Although the octarepeat constructs above provide quantitative K_d values for various binding modes, it is imperative that we re-evaluate components 1 and 2 in the intact octarepeat domain. We were not able to identify suitable chelators with K_d values in the micromolar range and therefore did not pursue competition studies, such as those used for component 3 binding (above). As an alternative, the direct measurement of the component 1 and 2 concentrations by EPR signal integration provides a means for determining the relevant binding equilibria. Specifically, a low concentration of PrP(23–28, 57–91) (<10 μM) was brought to equilibrium with 2.0 or more equivalents of Cu^{2+} (to avoid component 3 coordination), with EPR used to determine the concentrations of the free and bound species. Each sample was divided into two aliquots. Using the first aliquot, bound copper was measured by direct integration of the EPR spectrum. (Note that unbound, aqueous Cu^{2+} does not give an EPR spectrum; see the Discussion.) Total copper was determined by treating the second aliquot with a 10-fold excess of EDTA followed by signal integration. The difference between these two measurements gives the concentration of free Cu^{2+}. The resulting binding curve, with the corresponding fit to eq 1, is shown in Figure 4. The resulting K_d is 5.4 ± 2.0 μM. The examined concentrations correspond to a range in which there is a coexistence between components 1 and 2; therefore, this measured K_d cannot be assigned to either of the two specific binding modes and, instead, represents a composite value. The value of K_d measured this way is within experimental error of 7.2 μM measured for HGGGW (component 1) and a factor of 2 lower than that measured

for component 2. When these data are taken together, they again demonstrate that components 1 and 2 bind Cu^{2+} with low micromolar K_d values.

Cooperativity of Cu^{2+} Binding

As shown in our previous work, EPR spectra from a copper titration of PrP(23–28, 57–91) show a progression of different spectra and these are assigned to individual binding components (17). Component 3 dominates at low copper occupancy (≤1.0 equiv). Intermediate copper concentrations, in the range of 1.0–3.0 equiv, favor components 1 and 2, and higher concentrations give predominantly component 1, accompanied by a strong dipolar spectrum assigned to copper–copper couplings between individual component 1 modules (17). The proportion of each component, in conjunction with the copper affinity of each component, yields the change in affinity and binding cooperativity as a function of copper occupancy. This is evaluated below.

To determine the amount of each component as a function of total copper, experimental EPR spectra $S_{observed}$ are decomposed according to the relation

$$S_{\text{observed}} = \sum_i c_i S_i \tag{4}$$

where S_i are basis EPR spectra and c_i are coefficients proportional to the concentration of each component species. The basis set consists of normalized EPR spectra for components 1, 2, and 3 and dipolar-broadened component 1, shown in Figure 5A. The basis spectra were generated using the constructs in Table 1. A second basis spectrum for component 2 was obtained by subtraction of the component 1 portion from the EPR spectrum of a partially copper-occupied di-octarepeat peptide. This latter component 2 spectrum gave somewhat lower residuals when fitting to eq 4. The dipolar-broadened component 1 spectrum is from the EPR of a fully copper-occupied PrP(23–28, 57–91) with unbroadened component 1 subtracted. Fits using NNLS yield the coefficients, as well as the residual. The residual amplitudes are always less than 5% of the total signal, $S_{observed}$, and give no indication of additional spectral components beyond those in the fitting function. The resulting coefficients are shown plotted against total copper in Figure 5B.

Figure 5B shows how PrP(23–28, 57–91) passes through the various binding modes as a function of copper occupancy. Component 3 is essentially the only species observed when the copper occupancy is less than 1 equiv. With additional copper equivalents, component 3 diminishes, followed by the concomitant emergence of components 2 and 1. Beyond 2.0 equiv, component 1 dominates, as reflected by both its spectrum and the associated dipolar spectrum arising from strong coupling between component 1 modules.

Several previous studies suggest that PrP takes up copper with strong positive cooperativity, where the binding of each copper within an octarepeat domain increases the affinity for the next (8,22). Because of the progressive increase in affinity associated with positive cooperativity, copper-free and fully copper-occupied proteins should dominate the distribution of species, with only low concentrations of intermediates. Interestingly, the affinities determined for components 1, 2, and 3, along with the distribution shown in Figure 5B, argue against positive cooperativity. As opposed to a progressive increase in affinity, component 3, which takes up only a single Cu^{2+} per octarepeat domain, exhibits a higher affinity ($K_d \approx 0.1$ nM) than the multiple copper-occupied states reflected by component 2 ($K_d \approx 13\ \mu$M) and component 1 ($K_d \approx 7\ \mu$M). Moreover, Figure 5B shows that the population of intermediates is significant, with the singly copper-bound species dominating between 0.5 and 1.5 equiv.

To quantitate these findings, we determined the Hill coefficient, *n*, which serves as a phenomenological measure of binding cooperativity. A value of *n* greater than 1.0 corresponds to positive cooperativity; *n* less than 1.0 describes negative cooperativity. Noncooperative binding, where ligand-binding centers are fully independent of each other, follows $n = 1.0$. Derivation of the Hill coefficient requires the determination of the fraction of bound versus unbound copper throughout the titration curve (Figure 5B). Unfortunately, the acquisition of high-quality EPR spectra requires copper concentrations of at least 20 μM, a threshold that is beyond the K_d values reported above. As such, determining the fraction of unbound copper from the data in Figure 5B throughout the entire copper concentration range is not reliable. As an alternative, we use coupled equilibria, along with the measured K_d values, to provide approximate concentrations for all species. Specifically, the relevant set of reactions and corresponding equilibria are

$$\begin{aligned}
&\mathrm{PrP}+\mathrm{Cu}^{2+} \overset{K'_{d1}}{\longleftrightarrow} \mathrm{PrPCu}; \quad K'_{d1}=\frac{[\mathrm{PrP}][\mathrm{Cu}^{2+}]}{[\mathrm{PrPCu}]}=0.1\times10^{-9}\mathrm{M}\\
&\mathrm{PrPCu}+\mathrm{Cu}^{2+} \overset{K'_{d2}}{\longleftrightarrow} \mathrm{PrPCu_2}; \quad K'_{d2}=\frac{[\mathrm{PrPCu}][\mathrm{Cu}^{2+}]}{[\mathrm{PrPCu_2}]}=1.3\times10^{-5}\mathrm{M}\\
&\mathrm{PrPCu_2}+\mathrm{Cu}^{2+} \overset{K'_{d3}}{\longleftrightarrow} \mathrm{PrPCu_3}; \quad K'_{d3}=\frac{[\mathrm{PrPCu_2}][\mathrm{Cu}^{2+}]}{[\mathrm{PrPCu_3}]}=7\times10^{-6}\mathrm{M}\\
&\mathrm{PrPCu_3}+\mathrm{Cu}^{2+} \overset{K'_{d4}}{\longleftrightarrow} \mathrm{PrPCu_4}; \quad K'_{d4}=\frac{[\mathrm{PrPCu_3}][\mathrm{Cu}^{2+}]}{[\mathrm{PrPCu_4}]}=7\times10^{-6}\mathrm{M}
\end{aligned} \tag{5}$$

$$[\mathrm{Cu}^{2+}]_{\text{total bound}}=[\mathrm{PrPCu}]+2[\mathrm{PrPCu_2}]+3[\mathrm{PrPCu_3}]+4[\mathrm{PrPCu_4}] \tag{6}$$

We note that the copper occupancy of each species does not necessarily correspond to a specific binding mode. For example, the species $PrPCu_2$ may have both coppers bound as component 1, component 2, or a mixture of components 1 and 2 in the same octarepeat domain. Thus, the K_d' values in the equilibrium expressions above may be distinct from the K_d values for the individual binding modes. However, for the PrP octarepeat domain, the K_d' values may be assigned using the following observations. The first Cu^{2+} is taken up strictly as component 3 (Figure 5B), and occupancy of copper in this binding mode precludes component 1 or 2 binding in the same protein. K_{d1}' is therefore approximately equal to the K_d for component 3 (≈0.1 nM). In the vicinity of two equivalents, components 2 and 1 are observed in similar concentrations; therefore, K_{d2}' is set equal to the K_d for component 2, although K_{d2}' may be somewhat lower (but certainly no lower than 7 μM). Finally, all copper occupancy beyond 2 equiv is clearly dominated by component 1; therefore, the remaining K_d' values are set to 7 μM. Regardless of the specific K_d' values, beyond 2 equiv of copper, the measured K_d values exhibit little variation from approximately 10 μM, which places the values K_{d2}'–K_{d4}' also in the range of 10 μM.

The Hill coefficient is determined from the slope of log-(θ/(1 − θ)) versus log[Cu^{2+}], where θ is the fraction of copper-bound peptide (26). The coefficient is plotted as a function of θ in Figure 6. The resulting curve shows a significant variation with $n < 1.0$ throughout most of the concentration range and $n = 0.74$ at $\theta = 0.5$. Thus, in contrast to reports of positive cooperativity, the affinity data here suggest strong negative cooperativity for low copper occupancy (n_{min} = 0.2), with a shift to *n* slightly greater than 1.0 for for higher occupancy (n_{max} = 1.2).

Our findings are in contrast to the large Hill coefficients, in the range of 2.8–3.8, which have been reported for Cu^{2+} binding to PrP based on CD, fluorescence, and equilibrium dialysis

experiments (8,22,25). For example, the amplitude of the CD signal from PrP(58–91) at 570 nm gives a sigmoidal curve as a function of added copper, thus leading to the suggestion of strong positive cooperativity. Now with the identification of distinct binding components, the molar response of CD and other detection techniques to each binding mode becomes relevant and is further investigated here.

Cu^{2+} bound to peptides containing one or more octarepeats gives rise to CD signals with positive ellipticity at 340 and 590 nm, with the latter presumably because of weak d–d transitions. To determine how components 1, 2, and 3 individually contribute to this process, the CD spectra were recorded using the constructs in Table 1. The resulting spectra, shown in Figure 7, demonstrate that only component 1 is optically active at 590 nm. Therefore, CD spectra recorded in this spectral range only report component 1 copper binding and cannot be used to monitor total copper uptake or the degree of cooperativity. (Note the sigmoidal shape of the component 1 curve in Figure 5B.)

Fluorescence quenching studies on the octarepeat domain also give evidence of a sigmoidal curve, with a relatively flat response at low Cu^{2+} concentrations, suggesting positive cooperativity (22). To evaluate whether the copper-dependent binding components (Figure 1) are accountable for this response, the fluorescence quenching efficiency was measured for each of the constructs in Table 1. During measurements, excess copper was added to each of the PrP constructs to ensure full occupancy. Replicate measurements (data not shown) find that copper coordinated in the component 1 mode is approximately 1.5 times more effective at quenching Trp fluorescence than copper bound in the component 2 or 3 modes. This is probably due to the close proximity of the Trp indole in the component 1 copper coordination environment through its hydrogen bond to an axially bound water. It is therefore likely that the weaker quenching response of components 2 and 3, as opposed to positive cooperativity, is responsible for the sigmoidal fluorescence quenching curve observed for copper binding to the octarepeat domain.

Discussion

The octarepeat domain exhibits widely varying affinities for copper uptake, depending upon the specific Cu^{2+} coordination mode. At low occupancy, component 3 coordination dominates, characterized by a $K_d \approx 0.1$ nM. At high occupancy, component 1 takes over and binds with $K_d \approx 10\ \mu$M. Both HGGGW and the full octarepeat domain, represented by PrP(23–28, 57–91), possess micromolar K_d values for component 1 coordination. The variation in K_d between component 3 and component 1 coordination is nearly 5 orders of magnitude and consistent with negative cooperativity. Correspondingly, the Hill coefficient is significantly less than 1.0 throughout most of the copper concentration range.

The component 3 K_d was determined from direct competition experiments with well-characterized copper chelators. Moreover, EPR analysis ruled out any ternary complexes and assured that the only species in equilibrium were the copper-bound and unbound PrP and competitor. Consequently, the reported component 3 K_d is a robust value.

In contrast to the component 3 K_d evaluation, the component 1 and 2 K_d values were determined from equilibrium experiments with aqueous copper. Because of the complexity of copper equilibria in aqueous solution, we consider these K_d values as approximate. In aqueous solution, copper forms a number of different complexes, including copper hydroxides and copper chlorides. Both hydroxide and chloride ions have the capacity to bridge between copper ions, forming colloids; these colloids readily dissolve at lower pH or when challenged with copper-binding peptides. Anion bridging results in diamagnetic coupling between copper centers, thus eliminating the normal Cu^{2+} EPR signal (18). As noted in the Results, unbound

copper is EPR-silent, and this property facilitated our analysis of components 1 and 2 in PrP (23–28, 57–91). At pH 7.4, a dominant species is $Cu(OH)_2$, which is characterized by a solubility product of 2.2×10^{-20}. Using the OH^- concentration defined by pH 7.4, free copper arising from the equilibrium with copper hydroxide is approximately 0.4 μM. Consequently, the PrP constructs are not competing for free aqueous copper but instead for Cu^{2+} sequestered in colloids. The affinity of PrP for copper may be stronger than our K_d values suggest, and our reported values therefore represent upper bounds on the true dissociation constants for component 1 and 2 coordination. Despite this uncertainty, competition studies between PrP (23–28, 57–91), with a single equivalent of Cu^{2+}, and a 500-fold excess of HGGGW (see the Results) demonstrate no component 1 coordination whatsoever. Thus, component 3 coordination is, at a minimum, 3 orders of magnitude stronger than component 1 coordination. The component 1 K_d is therefore between 0.1 and 10 μM and most likely at the upper end of this range.

Because of the previously discussed complexities of working with full-length PrP (see the Results), our initial experiments focused on the isolated octarepeat domain. Clearly, the results reported here require not only confirmation in full-length PrP but also an assessment of the influence of non-octarepeat coordination sites (20,28) and other features that may affect Cu^{2+} uptake. With regard to octarepeat coordination, however, our previously published experiments on full-length PrP(29–231) suggest that the K_d values reported here are approximately correct (20). Specifically, we found that 21 μM PrP(29–231), when challenged with varying concentrations of Cu^{2+}, passed through the same intermediate species as PrP(23–28, 57–91). There was no evidence of a single high-affinity species that precluded micromolar affinity octarepeat binding, and component 1 coordination dominated only near full copper saturation. Thus, full-length PrP exhibits a wide range of copper affinities, up to the micromolar range, and shows negative cooperativity, just like isolated PrP(23–28, 57–91).

Since the discovery of the physiological connection of PrP to copper, there have been intensive efforts to determine the precise Cu^{2+} affinity (8,10,21–25). As noted in the Introduction, there is wide disagreement with reported K_d values distributed over nearly 8 orders of magnitude. At the time of these previous studies, however, it was not known that the PrP octarepeat domain binds Cu^{2+} with three coordination modes, depending upon the copper concentration. Moreover, several investigations, notably those that report extremely high copper affinity with near femtomolar K_d values, delivered Cu^{2+} as glycine chelates (21,22). Glycine and other Cu^{2+} bischelators present complex solution equilbria and allow for the formation of ternary complexes when in competition for copper bound in component 1 and 2 modes (EPR data not shown), which is certain to cloud the interpretation of binding data. Nevertheless, most determinations suggest micromolar dissociation constants, in agreement with our findings for component 1 coordination.

A fundamentally new and unique aspect of the work presented here is the finding that PrP takes up copper with strong negative cooperativity. Positive cooperativity, a familiar concept in the study of oxygen binding by hemoglobin, for example, allows a protein to respond to its ligand over a narrow concentration range. Negative cooperativity, on the other hand, spreads out this response over a wide concentration range. Interestingly, a recent survey of known cooperative enzymes finds that positive and negative cooperativity arise in the literature with approximately equal frequency (29). The consequence of negative cooperativity, in the PrP octarepeat domain, is that the protein transitions from 10 to 90% copper occupation over an extremely wide concentration range from 0.1 nM to 90 μM.

Numerous lines of evidence suggest that PrP functions as a neuroprotectant. Wild-type cells in culture are substantially more resistant to oxidative stress, arising from copper and other redox-active species, than PrP knockouts (14). Similarly, normal mice show much less tissue

oxidation than PrP knockouts (30). Although several mechanisms have been advanced to explain these observations, we have argued that the ability of component 1 coordination to quench copper redox activity is key (9,17). Because of the redox pair involving the oxidation states Cu^{+} and Cu^{2+}, high concentrations of weakly complexed copper contribute to the production of reactive oxygen species, which are toxic to cells. Component 1 coordination, however, binds specifically to Cu^{2+}, with a strong ligand field arising from the imidazole and deprotonated amide nitrogens, and preferentially stabilizes this oxidation state, thus reducing redox activity.

The prion protein is concentrated at presynaptic membranes (4). During neurotransmitter release, Cu^{2+} is released into the synaptic cleft. The best current estimates place the peak copper concentration in the range from 3.0 to 250 μM (31,32). At these concentrations, uncomplexed copper is likely to threaten cell viability. Thus, there must be mechanisms to protect against these transient copper concentration spikes. In blood and blood plasma, copper is buffered by amino acids, most of which are at micromolar concentrations (33), and serum albumin at a concentration of approximately 600 μM. Albumin takes up 1 equiv of copper in its N-terminal segment and, similar to PrP, coordinates in a fashion that stabilizes Cu^{2+} (although albumin has a much higher Cu^{2+} affinity than PrP). Cerebrospinal fluid (CSF) contains amino acids at concentrations similar to that found in blood. However, the concentration of albumin in CSF is approximately 100-fold lower than that in blood. Thus, while synapses experience significant changes in copper levels, with peak levels likely approaching 250 μM, the synaptic fluids themselves lack the ability to complex this cytotoxic species. Given that PrP responds to widely varying copper concentrations, resulting from negative cooperativity (mediated by component 3), and takes up copper in the concentration range found in synapses suggest that at least part of the function of PrP is to scavenge excess copper during neuronal activity. With the protein located at the presynaptic surface, it is positioned to hold onto copper until membrane transporters mobilize it back to the cell interior.

The cellular form of PrP is implicated in a number of critical neurophysiologic functions. Most certainly, at least one of these functions is related to the ability of the protein to take up Cu^{2+}. PrP responds to varying copper concentrations by passing through a series of distinct binding modes. Our results here show that K_d varies significantly as a function of copper occupation, resulting in pronounced negative cooperativity. The consequence is that the response of PrP is well-matched to Cu^{2+} variations in the synaptic cleft. Moreover, at high copper concentrations, in the micromolar range, PrP binds Cu^{2+} in a manner that quenches deleterious redox activity. This type of antioxidant function is likely to be key for the long-term maintenance of neurological tissues.

References

1. Prusiner SB. Prion diseases and the BSE crisis. Science 1997;278:245–251. [PubMed: 9323196]
2. Prusiner SB. Prions. Proc Natl Acad Sci U S A 1998;95:13363–13383. [PubMed: 9811807]
3. Prusiner, SB. Prion Biology and Diseases. 2nd. Cold Spring Harbor Laboratory Press; Cold Spring Harbor, NY: 2003.
4. Herms J, Tings T, Gall S, Madlung A, Giese A, Siebert H, Schürmann P, Windl O, Brose N, Kretzschmar H. Evidence of presynaptic location and function of the prion protein. J Neurosci 1999;19:8866–8875. [PubMed: 10516306]
5. Vassallo N, Herms J. Cellular prion protein function in copper homeostasis and redox signalling at the synapse. J Neurochem 2003;86:538–544. [PubMed: 12859667]
6. Donne DG, Viles JH, Groth D, Mehlhorn I, James TL, Cohen FE, Prusiner SB, Wright PE, Dyson HJ. Structure of the recombinant full-length hamster prion protein PrP(29–231): The N-terminus is highly flexible. Proc Natl Acad Sci U S A 1997;94:13452–13456. [PubMed: 9391046]

7. Inestrosa NC, Cerpa W, Varela-Nallar L. Copper brain homeostasis: Role of amyloid precursor protein and prion protein. IUBMB Life 2005;57:645–650. [PubMed: 16203684]
8. Brown DR, Qin K, Herms JW, Madlung A, Manson J, Strome R, Fraser PE, Kruck T, von Bohlen A, Schulz-Schaeffer W, Giese A, Westway D, Kretzschmar H. The cellular prion protein binds copper in vivo. Nature 1997;390:684–687. [PubMed: 9414160]
9. Millhauser GL. Copper binding in the prion protein. Acc Chem Res 2004;37:79–85. [PubMed: 14967054]
10. Whittal RM, Ball HL, Cohen FE, Burlingame AL, Prusiner SB, Baldwin MA. Copper binding to octarepeat peptides of the prion protein monitored by mass spectrometry. Protein Sci 2000;9:332–343. [PubMed: 10716185]
11. Pauly PC, Harris DA. Copper stimulates endocytosis of the prion protein. J Biol Chem 1998;273:33107–33119. [PubMed: 9837873]
12. Drisaldi B, Coomaraswamy J, Mastrangelo P, Strome B, Yang J, Watts JC, Chishti MA, Marvi M, Windl O, Ahrens R, Major F, Sy MS, Kretzschmar H, Fraser PE, Mount HT, Westaway D. Genetic mapping of activity determinants within cellular prion proteins: N-Terminal modules in PrPC offset pro-apoptotic activity of the Doppel helix B/B′ region. J Biol Chem 2004;279:55443–55454. [PubMed: 15459186]
13. Roucou X, Gains M, LeBlanc AC. Neuroprotective functions of prion protein. J Neurosci Res 2004;75:153–161. [PubMed: 14705136]
14. Brown DR, Schmidt B, Kretzschmar HA. Effects of copper on survival of prion protein knockout neurons and glia. J Neurochem 1998;70:1686–1693. [PubMed: 9523587]
15. Kanaani J, Prusiner SB, Diacovo J, Baekkeskov S, Legname G. Recombinant prion protein induces rapid polarization and development of synapses in embryonic rat hippocampal neurons in vitro. J Neurochem 2005;95:1373–1386. [PubMed: 16313516]
16. Brown DR, Wong BS, Hafiz F, Clive C, Haswell SJ, Jones IM. Normal prion protein has an activity like that of superoxide dismutase. Biochem J 1999;344:1–5. [PubMed: 10548526]
17. Chattopadhyay M, Walter ED, Newell DJ, Jackson PJ, Aronoff-Spencer E, Peisach J, Gerfen GJ, Bennett B, Antholine WE, Millhauser GL. The octarepeat domain of the prion protein binds Cu(II) with three distinct coordination modes at pH 7.4. J Am Chem Soc 2005;127:12647–12656. [PubMed: 16144413]
18. Aronoff-Spencer E, Burns CS, Avdievich NI, Gerfen GJ, Peisach J, Antholine WE, Ball HL, Cohen FE, Prusiner SB, Millhauser GL. Identification of the Cu^{2+} binding sites in the N-terminal domain of the prion protein by EPR and CD spectroscopy. Biochemistry 2000;39:13760–13771. [PubMed: 11076515]
19. Burns CS, Aronoff-Spencer E, Dunham CM, Lario P, Avdievich NI, Antholine WE, Olmstead MM, Vrielink A, Gerfen GJ, Peisach J, Scott WG, Millhauser GL. Molecular features of the copper binding sites in the octarepeat domain of the prion protein. Biochemistry 2002;41:3991–4001. [PubMed: 11900542]
20. Burns CS, Aronoff-Spencer E, Legname G, Prusiner SB, Antholine WE, Gerfen GJ, Peisach J, Millhauser GL. Copper coordination in the full-length, recombinant prion protein. Biochemistry 2003;42:6794–6803. [PubMed: 12779334]
21. Thompsett AR, Abdelraheim SR, Daniels M, Brown DR. High affinity binding between copper and full-length prion protein identified by two different techniques. J Biol Chem 2005;280:42750–42758. [PubMed: 16258172]
22. Kramer ML, Kratzin HD, Schmidt B, Romer A, Windl O, Liemann S, Hornemann S, Kretzschmar H. Prion protein binds copper within the physiological concentration range. J Biol Chem 2001;276:16711–16719. [PubMed: 11278306]
23. Garnett AP, Viles JH. Copper binding to the octarepeats of the prion protein. Afffinity, specificity, folding and cooperativity: Insights from circular dichroism. J Biol Chem 2003;278:6795–6802. [PubMed: 12454014]
24. Jackson GS, Murray I, Hosszu LLP, Gibbs N, Waltho JP, Clarke AR, Collinge J. Location and properties of metal-binding sites on the human prion protein. Proc Natl Acad Sci U S A 2001;98:8531–8535. [PubMed: 11438695]

25. Viles JH, Cohen FE, Prusiner SB, Goodin DB, Wright PE, Dyson HJ. Copper binding to the prion protein: Structural implications of four identical cooperative binding sites. Proc Natl Acad Sci U S A 1999;96:2042–2047. [PubMed: 10051591]

26. Cantor, CR.; Schimmel, PR. Biophysical Chemistry. W. H. Freeman; San Francisco, CA: 1980.

27. Shields SB, Franklin SJ. De novo design of a copper(II)-binding helix–turn–helix chimera: The prion octarepeat motif in a new context. Biochemistry 2004;43:16086–16091. [PubMed: 15610003]

28. Qin K, Yang Y, Mastrangelo P, Westaway D. Mapping Cu(II) bindings sites in prion proteins by diethylpyrocarbonate modification and MALDI–TOF mass spectrometric “footprinting”. J Biol Chem 2002;277:1981–1990. [PubMed: 11698407]

29. Koshland DE Jr, Hamadani K. Proteomics and models for enzyme cooperativity. J Biol Chem 2002;277:46841–46844. [PubMed: 12189158]

30. Klamt F, Dal-Pizzol F, Conte DA, Frota ML Jr, Walz R, Andrades ME, Gomes DA, Silva E, Brentani RR, Izquierdo I, Moreira JCF. Imbalance of antioxidant defense in mice lacking cellular prion protein. Free Radical Biol Med 2001;30:1137–1144. [PubMed: 11369504]

31. Hopt A, Korte S, Fink H, Panne U, Niessner R, Jahn R, Kretzschmar H, Herms J. Methods for studying synaptosomal copper release. J Neurosci Methods 2003;128:159–172. [PubMed: 12948559]

32. Kardos J, Kovacs I, Hajos F, Kalman M, Simonyi M. Nerve endings from rat brain tissue release copper upon depolarization. A possible role in regulating neuronal excitability. Neurosci Lett 1989;103:139–144. [PubMed: 2549468]

33. May PM, Linder PW, Williams DR. Computer simulation of metal-ion equilibria in biofluids: Models for the low-molecular-weight complex distribution of calcium(II), magnesium(II), manganese(II), iron(III), copper(II), zinc(II), and lead-(II) ions in human blood plasma. J Chem Soc, Dalton Trans 1977:588–595.

34. Dawson, RMC.; Elliot, DC.; Elliot, DH.; Jones, KM. Data for Biochemical Research. 3rd. Oxford University Press; Oxford, U.K.: 1986. p. 408-410.

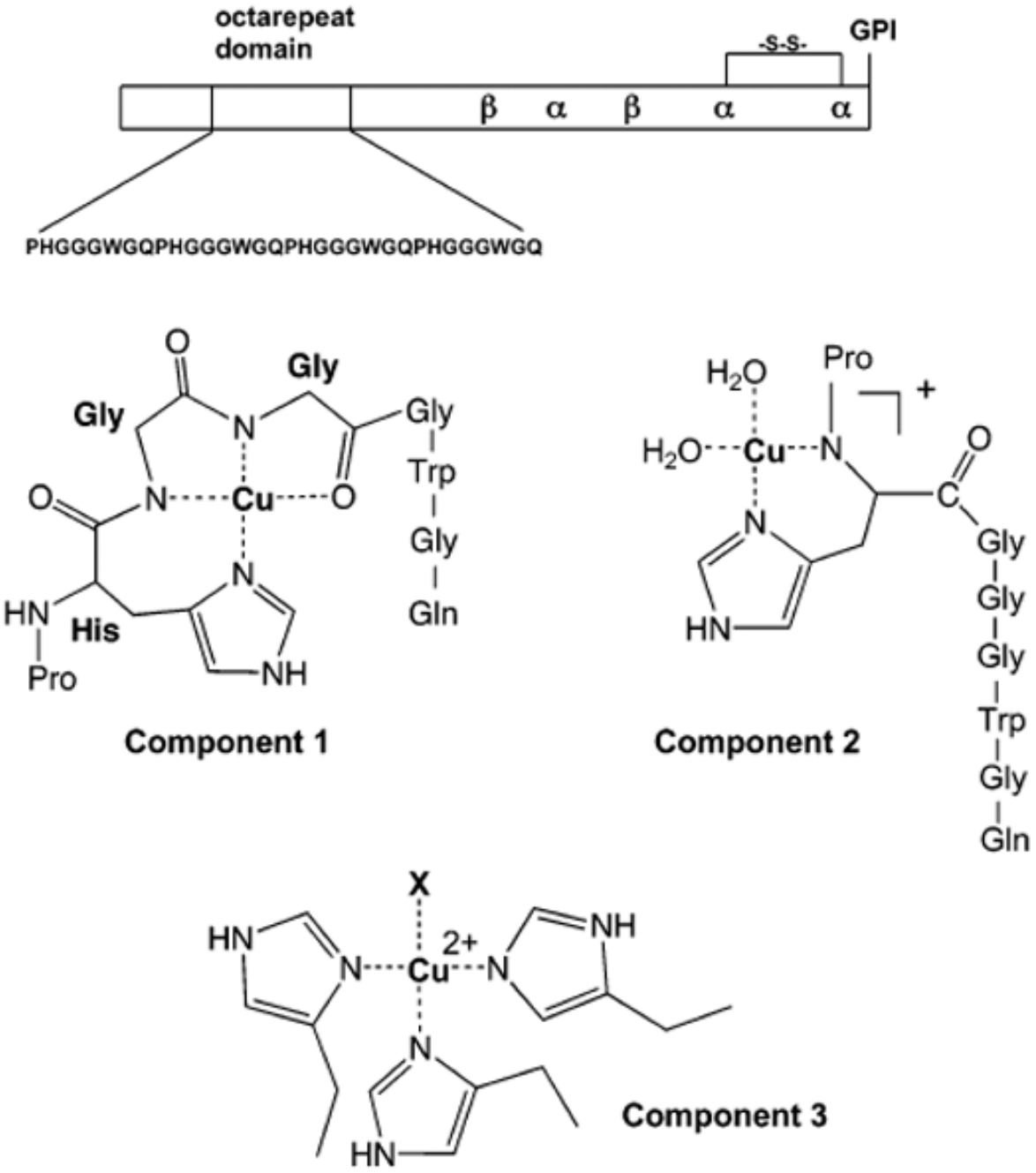

Figure 1.

PrP possesses a flexible N-terminal domain and a globular C-terminal domain, made up of three R helices and two β strands, as shown above. Copper binds primarily in the octarepeat domain, composed of tandem repeats of the fundamental sequence PHGGGWGQ. Other notable features are the disulfide bond that links two C-terminal helices and the GPI anchor, which tethers PrP to cellular membranes. Cu^{2+} binds in the octarepeat domain with three different coordination modes, as shown. Component 3 dominates at low Cu^{2+} occupancy, and component 1 dominates at saturation.

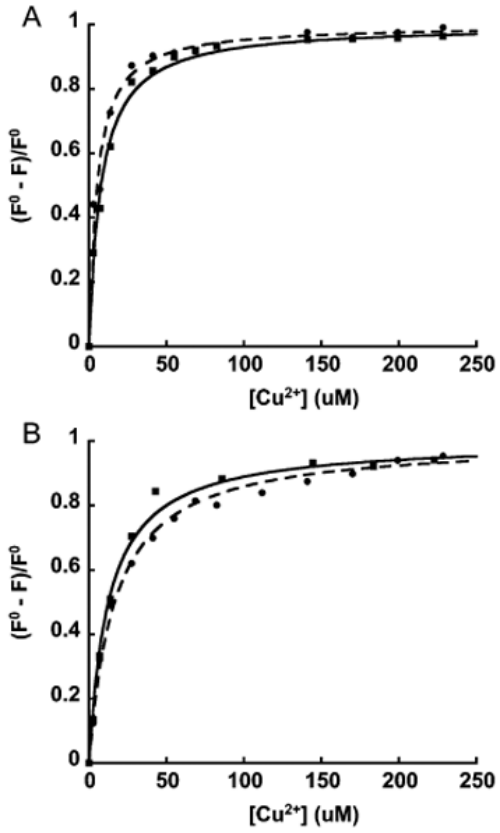

Figure 2.

Tryptophan fluorescence quenching from Cu^{2+} for determining the copper K_d for (A) component 1 and (B) component 2, using the appropriate octarepeat constructs in Table 1. For each case, two representative curves are shown, corresponding to peptide concentrations of 1.0 μM (●) and 5.0 μM (■). The solid lines are fits to eq 1.

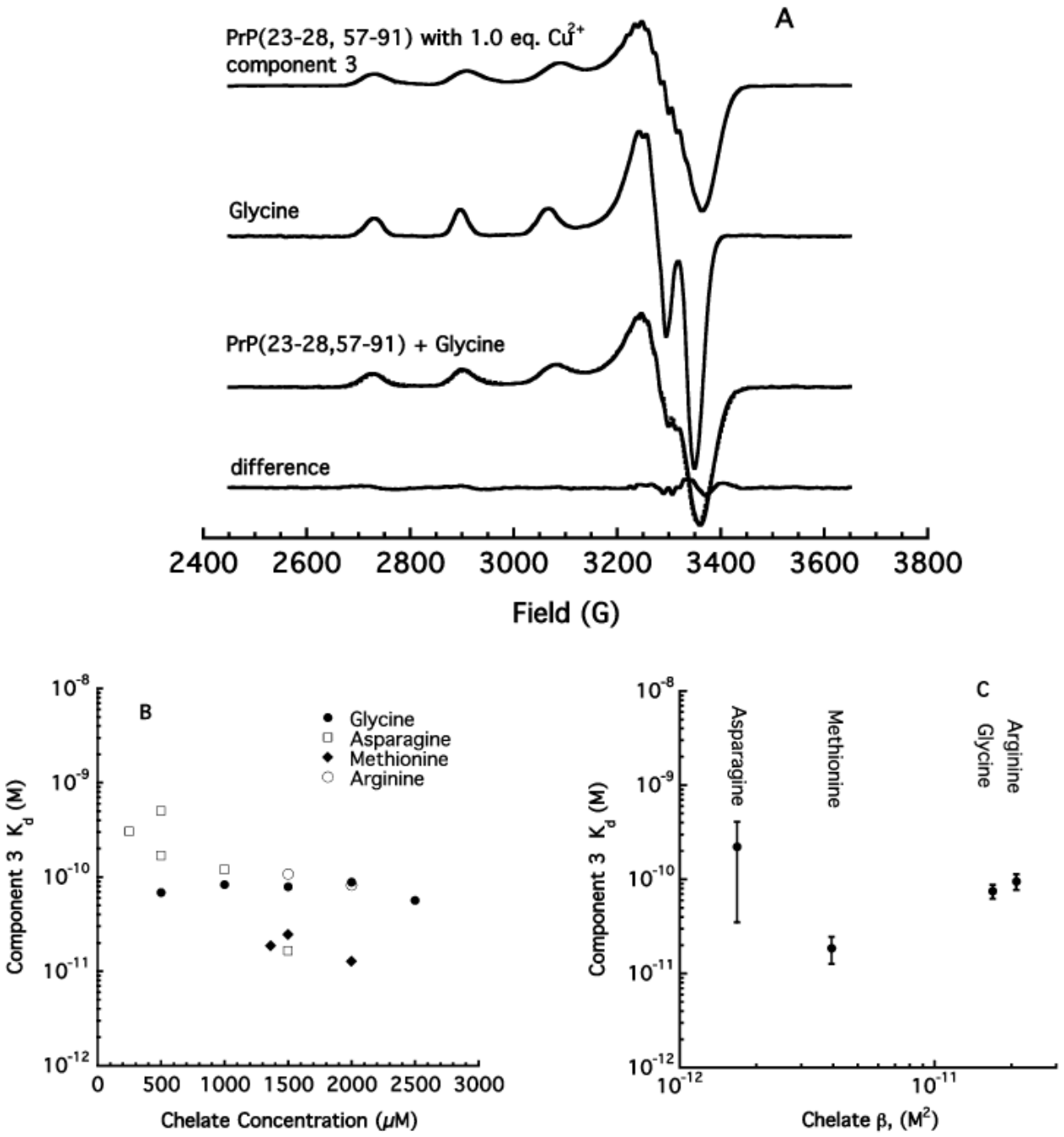

Figure 3.

Copper competition experiments, using a selection of amino acid chelators and detected by EPR, to determine the component 3 K_d. (A) Top two spectra are Cu^{2+} complexes of PrP(23–28, 57–91) and glycine, respectively. Next is the spectrum from a mixture of PrP(23–28, 57–91) (250 μM) and glycine (2.5 mM), with a limiting amount of Cu^{2+}. The solid line shows the experimental spectrum, and the dashed line shows the fit to a superposition of the two spectra above [15% glycine plus 85% PrP(23-28, 57-91)]. The bottom is the difference between the experimental and the fit. (B) Measured K_d values for four amino acids as a function of their concentrations. (C) Average K_d values for each of the amino acid chelators as a function of

their dissociation constants, β. B and C demonstrate that measured K_d values for component 3 are relatively independent of the chosen chelator or its concentration.

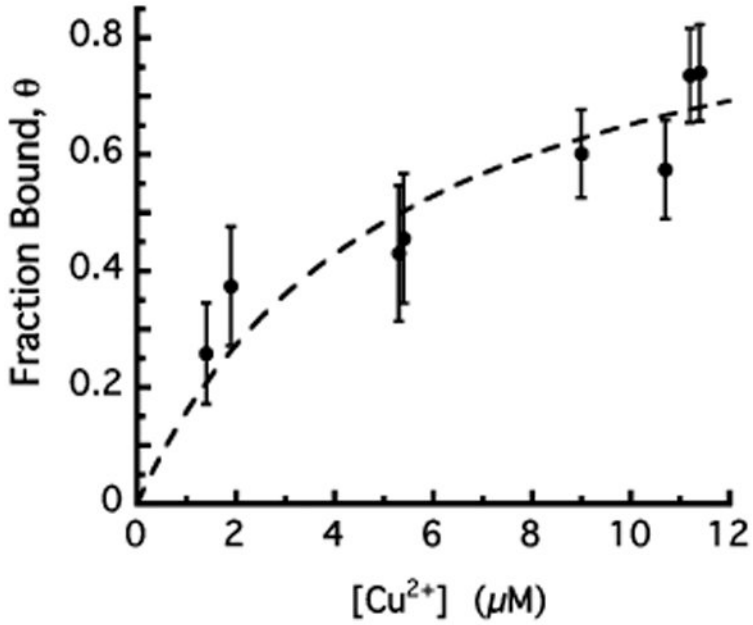

Figure 4.

Binding curve, detected by EPR, for component 1 and 2 coordination in PrP(23–28, 57–91). K_d is 5.4 ± 2.0 μM, which matches well to K_d values for these coordination modes using shorter octarepeat constructs and determined by fluorescence quenching (Figure 2).

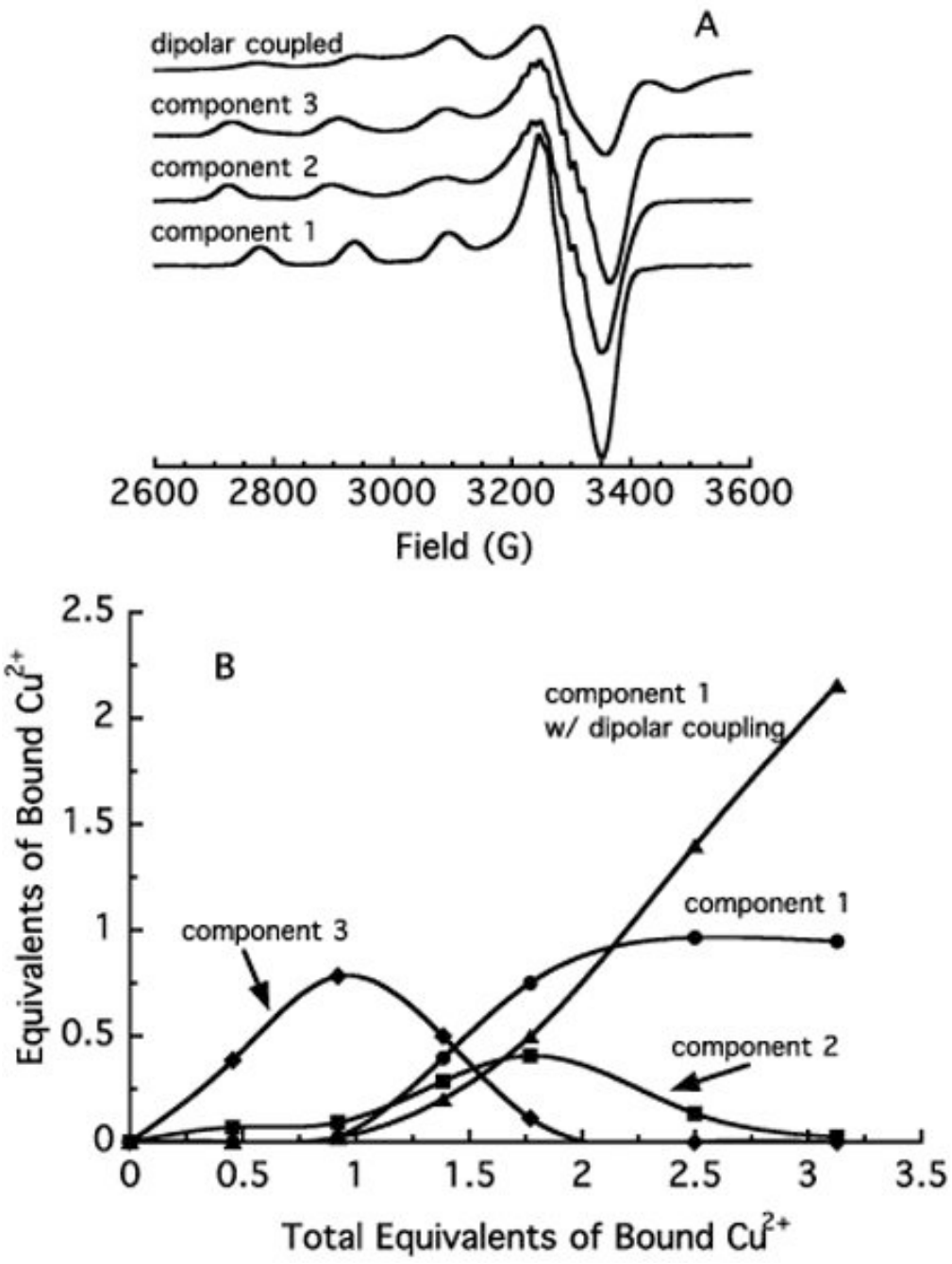

Figure 5.

(A) EPR basis spectra of the individual coordination modes. The dipolar coupled spectrum occurs at full copper occupancy of PrP(23–28, 57–91) and arises from copper–copper couplings between component 1 centers. All spectra are normalized to the same Cu^{2+} concentration. (B) Relative populations of components 1, 2, and 3 as a function of the total bound Cu^{2+}. The significant population of intermediate species, such as component 3, is consistent with negative cooperativity.

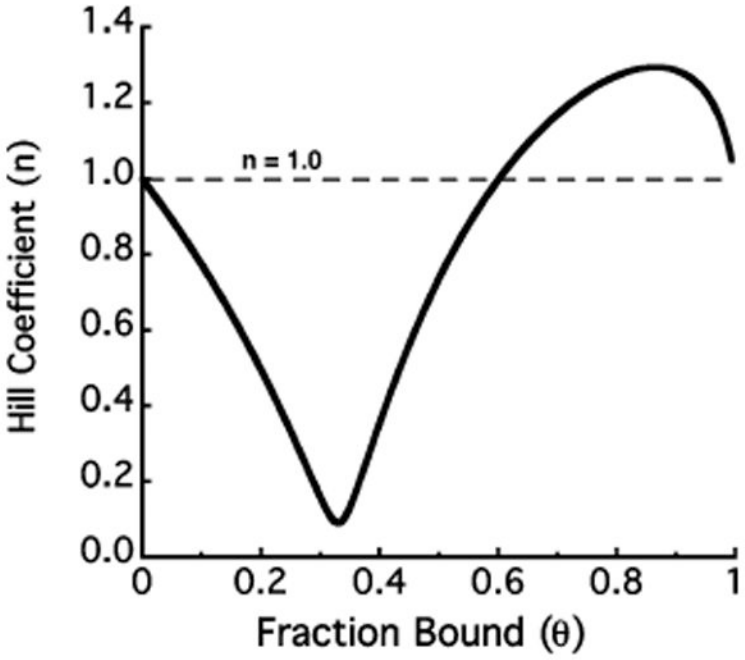

Figure 6.
Measured Hill coefficient, *n*, as a function of the fraction of PrP(23–28, 57–91) bound with Cu^{2+}. Over most of the range, *n* is less than 1.0 (- - -), which demonstrates negative cooperativity.

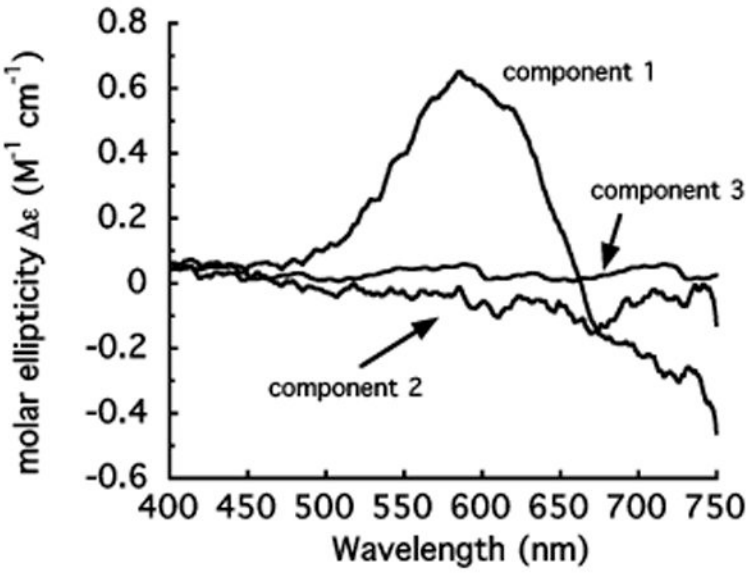

Figure 7.
CD spectra for the various copper-binding modes. Only component 1 is CD-active in the visible range. Component 1 becomes populated only beyond 1.0 equiv of copper (Figure 5), which explains why CD measurements report sigmoidal binding curves.

Table 1

Peptide Sequences[a]

$KKRPKPWGQ(PHGGGWGQ)_4$	PrP(23–28, 57–91)
HGGGWGQPHGGGW	
HGGGW	
HGXGWGQPHGXGW	

[a] X = sarcosine (*N*-methylglycine).

Table 2

Dissociation Constants, K_d[a]

sequence	0.5 μM[b]	1.0 μM	2.0 μM	5.0 μM	K_d (mean)	SD[c]
HGGGW	6.7	5.1	9.2	7.7	7.2	2.8
HGXGWGQPHGXGW	11.8	15.0	11.0	12.8	12.6	2.6

[a] All K_d values are reported in micromolar.

[b] Peptide concentrations.

[c] SD = standard deviation.

Table 3

Amino Acid K_d Values[a]

	K_{dc1}	K_{dc2}	β
arginine	1.2×10^{-6} M	1.8×10^{-5} M	2.1×10^{-11} M^2
asparagine	2.8×10^{-7} M	6.0×10^{-6} M	1.7×10^{-12} M^2
glycine	1.3×10^{-6} M	1.3×10^{-5} M	1.7×10^{-11} M^2
methionine	5.0×10^{-7} M	7.9×10^{-6} M	4.0×10^{-12} M^2

[a]From ref 34.